Title

An unexpected catalyst dominates formation and radiative forcing of regional haze

Journal

Proceedings of the National Academy of Sciences of the United States of America, 117(8)

ISSN

0027-8424

Authors

Zhang, Fang
Wang, Yuan
Peng, Jianfei
et al.

Publication Date

2020-02-25

DOI

10.1073/pnas.1919343117

Peer reviewed

An unexpected catalyst dominates formation and radiative forcing of regional haze

Fang Zhang[a,b], Yuan Wang[c], Jianfei Peng[b], Lu Chen[a], Yele Sun[d], Lian Duan[b,e], Xinlei Ge[f], Yixin Li[g], Jiayun Zhao[g], Chao Liu[h], Xiaochun Zhang[i,j], Gen Zhang[i,j], Yuepeng Pan[d], Yuesi Wang[d], Annie L. Zhang[k], Yuemeng Ji[l], Gehui Wang[m], Min Hu[n], Mario J. Molina[o,1], and Renyi Zhang[b,g,1]

[a]College of Global Change and Earth System Science, Beijing Normal University, 100875 Beijing, China; [b]Department of Atmospheric Sciences, Texas A&M University, College Station, TX 77843; [c]Division of Geological and Planetary Sciences, California Institute of Technology, Pasadena, CA 91125; [d]State Key Laboratory of Atmospheric Boundary Layer Physics and Atmospheric Chemistry, Institute of Atmospheric Physics, Chinese Academy of Sciences, 100080 Beijing, China; [e]State Environmental Protection Key Lab of Environmental Risk Assessment and Control on Chemical Processes, East China University of Science and Technology, 200237 Shanghai, China; [f]Jiangsu Key Laboratory of Atmospheric Environment Monitoring and Pollution Control, Nanjing University of Information Science and Technology, 210044 Nanjing, China; [g]Department of Chemistry, Texas A&M University, College Station, TX 77843; [h]School of Atmospheric Physics, Nanjing University of Information Science & Technology, 210044 Nanjing, China; [i]State Key Laboratory of Severe Weather, Chinese Meteorological Administration, Chinese Academy of Meteorological Sciences, 100081 Beijing, China; [j]Key Laboratory of Atmospheric Chemistry, Chinese Meteorological Administration, Chinese Academy of Meteorological Sciences, 100081 Beijing, China; [k]Department of Chemistry, College of Natural Sciences, The University of Texas at Austin, Austin, TX 78712; [l]Guangzhou Key Laboratory of Environmental Catalysis and Pollution Control, School of Environmental Science and Engineering, Institute of Environmental Health and Pollution Control, Guangdong University of Technology, 510006 Guangzhou, China; [m]Key Laboratory of Geographic Information Science of the Ministry of Education, School of Geographic Sciences, East China Normal University, 200241 Shanghai, China; [n]State Key Joint Laboratory of Environmental Simulation and Pollution Control, College of Environmental Sciences and Engineering, Peking University, 100871 Beijing, China; and [o]Department of Chemistry and Biochemistry, University of California San Diego, La Jolla, CA 92093

Contributed by Mario J. Molina, December 24, 2019 (sent for review November 7, 2019; reviewed by Russell R. Dickerson and Manish Shrivastava)

Although regional haze adversely affects human health and possibly counteracts global warming from increasing levels of greenhouse gases, the formation and radiative forcing of regional haze on climate remain uncertain. By combining field measurements, laboratory experiments, and model simulations, we show a remarkable role of black carbon (BC) particles in driving the formation and trend of regional haze. Our analysis of long-term measurements in China indicates declined frequency of heavy haze events along with significantly reduced SO_2, but negligibly alleviated haze severity. Also, no improving trend exists for moderate haze events. Our complementary laboratory experiments demonstrate that SO_2 oxidation is efficiently catalyzed on BC particles in the presence of NO_2 and NH_3, even at low SO_2 and intermediate relative humidity levels. Inclusion of the BC reaction accounts for about 90–100% and 30–50% of the sulfate production during moderate and heavy haze events, respectively. Calculations using a radiative transfer model and accounting for the sulfate formation on BC yield an invariant radiative forcing of nearly zero W m^{-2} on the top of the atmosphere throughout haze development, indicating small net climatic cooling/warming but large surface cooling, atmospheric heating, and air stagnation. This BC catalytic chemistry facilitates haze development and explains the observed trends of regional haze in China. Our results imply that reduction of SO_2 alone is insufficient in mitigating haze occurrence and highlight the necessity of accurate representation of the BC chemical and radiative properties in predicting the formation and assessing the impacts of regional haze.

black carbon | air pollution | climate | multiphase chemistry | haze

Because of rapid urbanization, industrialization, and economic growth, many developing countries have experienced frequent haze pollution (1–4), which profoundly impacts human health, weather, and climate (5–9). Noticeably, air quality in the developing world moves along a trajectory that had been previously encountered in most developed countries (1, 4). Air quality is inherently controlled by the synergetic effects of emissions, chemistry, transport, and removal of pollutants (1, 4). While atmospheric circulation is likely subjected to the influence of climate change, fine aerosols also exert direct and indirect feedbacks to climate, via the aerosol–radiation interaction (ARI) and aerosol–cloud interaction, respectively (8–11). Regional haze, which is characterized by high levels of fine aerosols with large spatial and temporal coverage, occurs frequently in Asia, such as China and India (1–4). For example, a month-long haze extreme in January 2013 covered more than 10% (1.3 million km^2) of the territory and affected more than 50% (about 800 million) of the population in China (4).

Improved understanding of the chemical/physical processes leading to haze formation is crucial to devising effective mitigation strategies to protect the public and reduce uncertainties in climate predictions (5–7). The frequent occurrence of severe haze in China has prompted a variety of legislative actions for air-quality improvement, which have resulted in significantly

Significance

Regional haze adversely affects human health and possibly counteracts global warming by greenhouse gases, but its formation and radiative forcing remain unclear. Here we present field measurements to show reduced frequency but not severity for heavy haze and little-improved moderate haze, when SO_2 is significantly reduced in China. Our laboratory experiments identify black carbon (BC)-catalyzed sulfate formation involving NO_2 and NH_3. Radiative transfer calculations accounting for this BC chemistry indicate small net climatic cooling/warming but large surface cooling, atmospheric heating, and air stagnation. Our work reveals that this BC catalytic chemistry dominates the formation, trend, and radiative forcing of regional haze, suggesting the necessity of simultaneous reduction in emissions of SO_2, NO_x, NH_3, and BC for air-quality improvement.

Author contributions: F.Z. and R.Z. designed research; F.Z., Yuan Wang, J.P., L.C., Y.S., and R.Z. performed research; X.G., X.Z., G.Z., Y.P., Yuesi Wang, M.H., and M.J.M. contributed new reagents/analytic tools; F.Z., J.P., Y.S., L.D., Y.L., J.Z., C.L., Y.J., G.W., and M.J.M. analyzed data; and F.Z., A.L.Z., and R.Z. wrote the paper.

Reviewers: R.R.D., University of Maryland; and M.S., Pacific Northwest National Laboratory.

The authors declare no competing interest.

[1]To whom correspondence may be addressed. Email: mjmolina@ucsd.edu or renyi-zhang@tamu.edu.

This article contains supporting information online at https://www.pnas.org/lookup/suppl/doi:10.1073/pnas.1919343117/-/DCSupplemental.

First published February 10, 2020.

reduced emissions of SO_2 and primary aerosols (1, 4). Satellite top-down estimates showed decreased SO_2 emissions from over 30 Mt y^{-1} in 2005 to less than 10 Mt y^{-1} in 2016 (4, 12). However, the effectiveness of most regulatory policies has yet to be rigorously evaluated, and implementation of regulatory measures without a scientific basis may also incur undesirable consequences (1, 4). Specifically, it has been suggested that regional haze may be effectively minimized by controlling NH_3 emission, but reduction of NH_3 without simultaneously regulating emissions of SO_2 and NO_2 likely poses a threat for the occurrence of highly acidic haze events, analogous to the catastrophic 1952 London Fog (13, 14). Also, while lower levels of air pollutants benefit the public health, most climate models showed that the shield of sunlight by fine aerosols (mainly ARI associated with sulfate, nitrate, and organics) has kept the planet cooler by as much as 0.7 °C globally, suggesting that reduction in aerosol pollution likely accelerates global warming (15). In addition, the black carbon (BC) direct radiative forcing represents another central issue on climate, because the global solar absorption by BC is estimated to be as much as 0.9 W m^{-2}, second only to that by carbon dioxide (16, 17). Currently, large uncertainties exist on BC optical properties, since its ability to absorb light varies considerably during atmospheric processes (18, 19). Under polluted environments, rapid aging of BC particles results in significantly enhanced surface cooling/atmospheric heating and consequently diminished diurnal variation of the atmospheric planetary boundary layer (PBL) and exacerbates haze development (10, 20). In this work, we evaluated the underlying mechanisms for regional haze formation by combining field measurements, laboratory experiments, and model simulations (*Methods*).

Field and Laboratory Measurements

We analyzed long-term measurements of $PM_{2.5}$, sulfate, BC, and gaseous concentrations of SO_2, NO_2, and NH_3 in the Northern China Plain (NCP). In our work, air quality was categorized as clean/light haze, moderate haze, and heavy haze conditions, with the corresponding daily mean $PM_{2.5}$ (particulate matter smaller than 2.5 μm) mass concentrations of <100, 100–200, and >200 μg m^{-3}, respectively (Figs. 1 and 2*A*). Haze occurrence in NCP exhibits an improving trend since 2013 (Fig. 1*A*), as reflected by a decreasing number of heavy haze days and an increasing number of clean/light haze days. For example, the numbers of clean/light haze and heavy haze days are 176 and 58 in 2013 and 227 and 15 in 2018, respectively. On the other hand, there exists no obvious trend for moderate haze events with an average of 113 d from 2004 to 2018 and no improving trends for the daily average mass concentrations of $PM_{2.5}$ and sulfate during moderate and heavy haze days (Fig. 1 *B* and *C*). The decreasing (increasing) number of heavy (clean/light) haze days correlates to the SO_2 trend, which exhibits a constant decrease from 70 parts per billion (ppb) in 2013 to a few ppb in 2018 during heavy haze events (Fig. 1*E*). The declining SO_2 level is consistent with other ground-based and satellite measurements (4, 12). In addition, slightly decreasing trends in BC and NO_2 during moderate and heavy haze periods are evident in recent years (Fig. 1 *D* and *F*), while no apparent trend exists for NH_3 (*SI Appendix*, Fig. S1). Emissions of SO_2, NO_x, and BC in China are mainly associated with combustion from gasoline or diesel vehicles, residential sources, power plants, and industrial facilities (4). Satellite measurements showed that NH_3 emissions from agricultural sources increased substantially over China in recent years, because of increasing temperature and fertilizer use (21).

The declined frequency but not severity for heavy haze is mostly evident from recent measurements during the 2018–2019

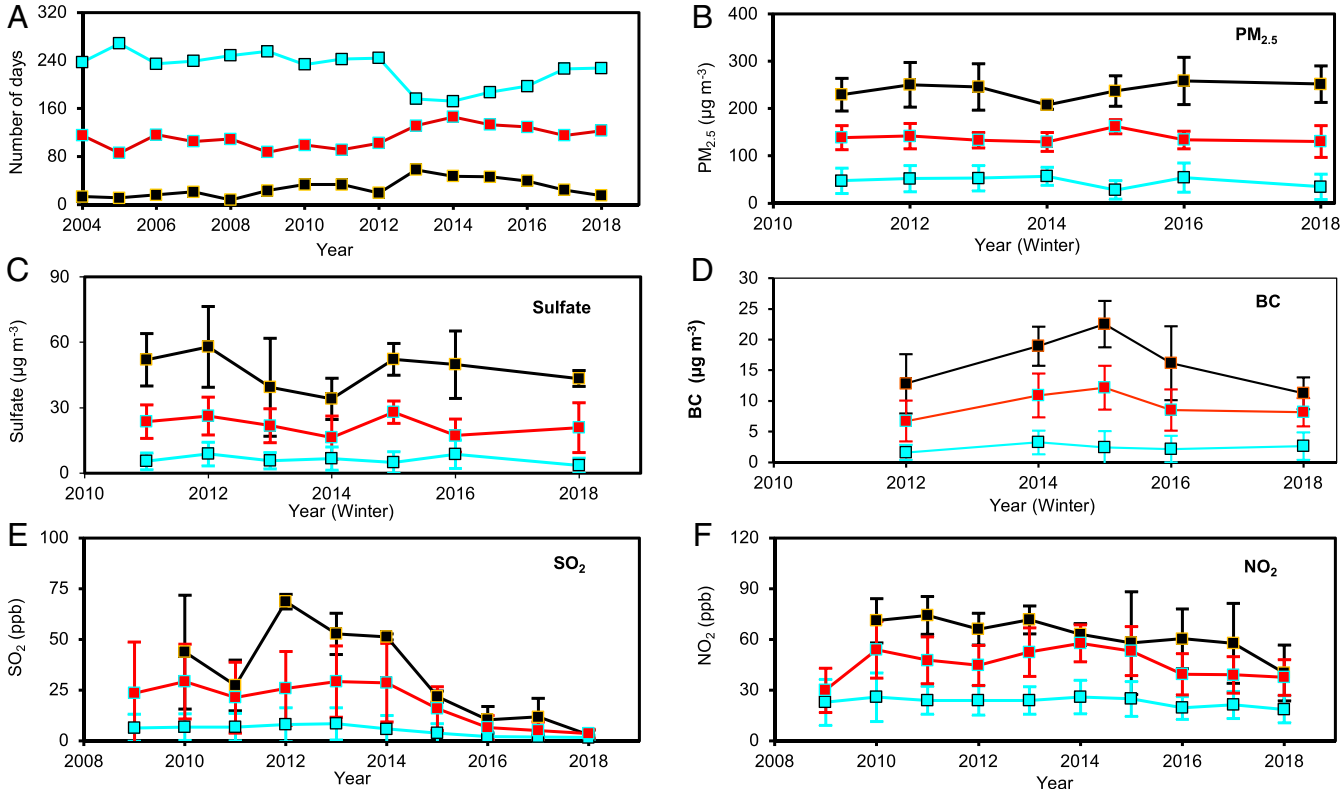

Fig. 1. Long-term trends of air quality in Beijing. (*A*) Trends of the numbers of clean/light haze (blue), moderate haze (red), and heavy haze (black) days since 2004. (*B–F*) Measurements of $PM_{2.5}$ (*B*), sulfate (*C*), BC (*D*), SO_2 (*E*), and NO_2 (*F*).

winter. There is a total number of 15 heavy haze events during this period, with the daily mean $PM_{2.5}$ and sulfate concentrations of 250 and 45 μg m^{-3}, respectively. For comparison, there are on average 29 heavy haze events, with the daily mean $PM_{2.5}$ and sulfate concentrations of 230 and 40 μg m^{-3}, respectively, during 2004–2018. Heavy haze typically develops with a sharp rise in the sulfate concentration, which occurs concurrently with elevated BC, NO_2, NH_3, and RH, even at a low SO_2 level (Fig. 2 *B* and *C*).

To elucidate the chemical mechanism leading to sulfate formation, we performed laboratory experiments by exposing fresh BC particles to variable levels of SO_2, NO_2, NH_3, and RH in a dark environmental chamber (*Methods*). Monodispersed BC particles with an initial size of 100–150 nm grow rapidly upon exposure to these gaseous species (Fig. 3), as quantified from the simultaneously measured size, mass, and light extinction/scattering (22, 23). Considerable mass growth (defined by *dGfm*/*dt*, where *Gfm* is the mass growth factor) occurs when BC particles are exposed simultaneously to SO_2, NO_2, and NH_3 (Fig. 3 *A*–*C*). The mass growth is insensitive to SO_2 in the range of 7–375 ppb (Fig. 3*A*), but depends strongly on the concentrations of NO_2 and NH_3 (Fig. 3 *B* and *C*). Also, the mass growth increases monotonically with RH in the range of 30–70% and exhibits a slight decreasing trend at high RH (>70%) (Fig. 3*D*). The BC mass growth is also accompanied by changes in the optical properties (Fig. 3*E*). The BC absorption (denoted by absorption enhancement, E_a) increases significantly on heavily coated (aged) particles. The mass absorption cross-section (*MAC*) increases from 7.5 to 12.8 m^2 g^{-1} for fresh and aged BC, respectively, with a corresponding E_a value of 1.7 (Fig. 3*E*). To identify the species responsible for the measured mass growth, we analyzed the particle chemical compositions using a thermal-desorption ion-drift chemical ionization mass spectrometer (TD-ID-CIMS) (24, 25). The contribution of sulfate formation to the particle growth is confirmed by significant presence of several sulfate-related ions, i.e., SO_4^{-2} at m/z = 96 and HSO_4^- at m/z = 97, on the exposed particles (Fig. 3*F*). In addition, there is negligible growth of BC particles in the absence of one of the three gaseous species (SO_2, NO_2, or NH_3) or at low RH (<10%), suggesting that SO_2, NO_2, NH_3, and H_2O are indispensable to sulfate production on BC particles. The sulfate formation on BC is distinct from a previously proposed mechanism that involves aqueous SO_2 oxidation by NO_2 with NH_3 neutralization at high RH (>70%) (13, 14). The BC-catalytic chemistry involves the initial production of nitrous acid (HONO) from the reaction of NO_2 on BC and subsequent aqueous reactions with hydrogen sulfite/bisulfite ions to yield sulfate. Uptake of NO_2 occurs through physical adsorption at BC surface sites, {S}, and HONO formation occurs via extraction of an allylic hydrogen by NO_2 at reducing

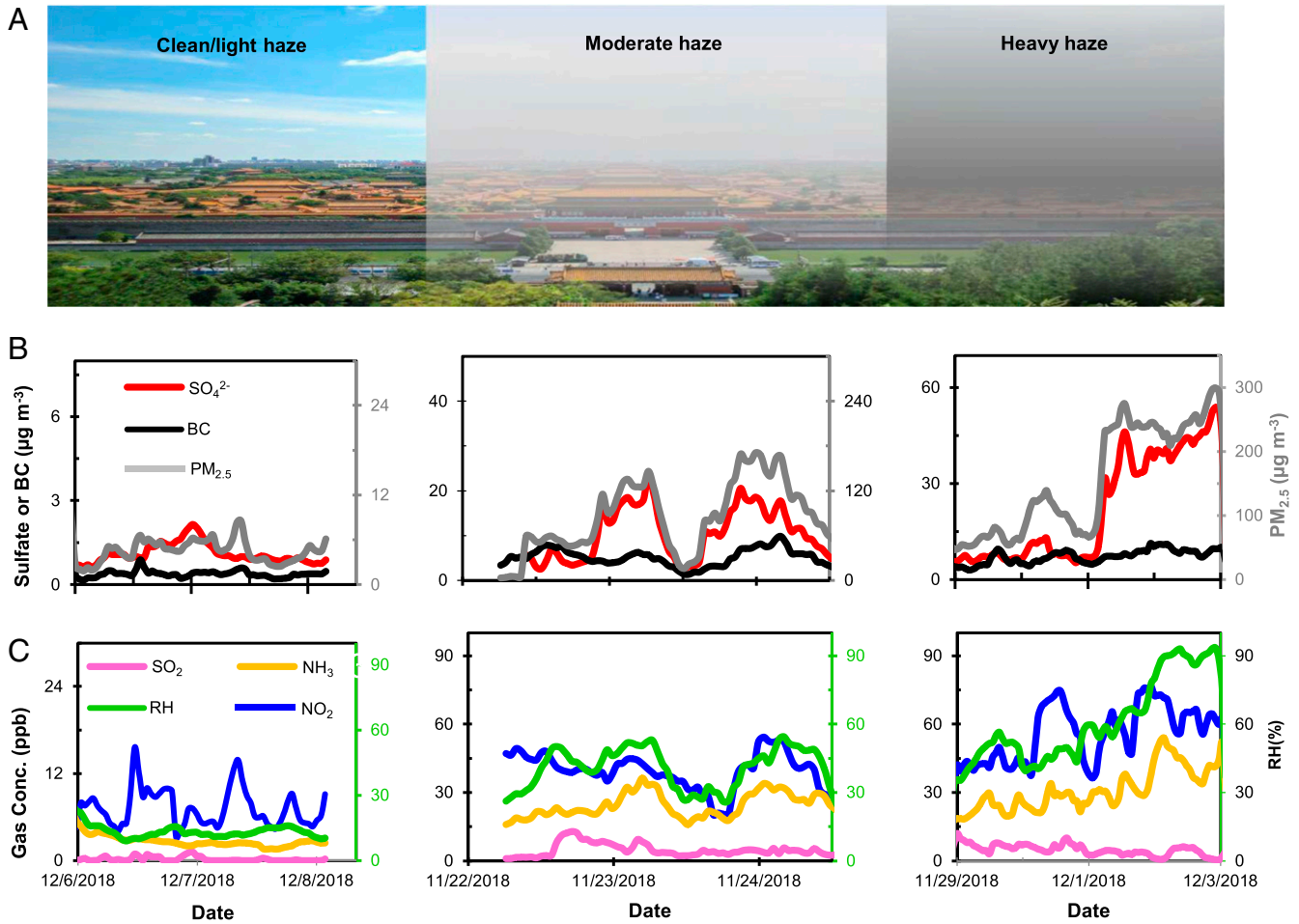

Fig. 2. An update of air quality from Beijing: no alleviated haze severity. (*A*) Pictures of the Forbidden City in Beijing during clean/light haze, moderate haze, and heavy haze periods. (*B*) Measurements of sulfate/BC (*Left* axis) and $PM_{2.5}$ (*Right* axis) mass concentrations during evolutions for clean/light haze (*Left*), moderate haze (*Middle*), and heavy haze (*Right*) episodes in Beijing. (*C*) Measurements of gaseous SO_2/NO_2/NH_3 (*Left* axis) and RH (*Right* axis) during the similar period as in *B*.

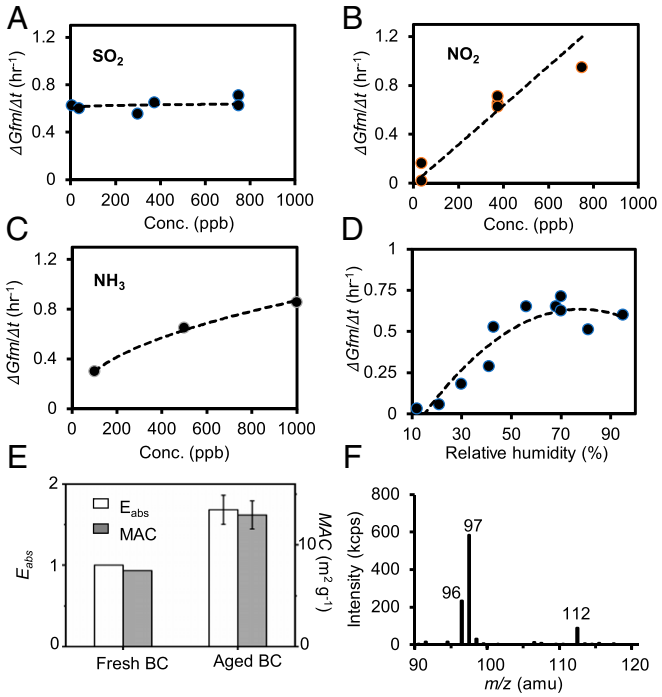

Fig. 3. BC-catalyzed sulfate formation. (*A–D*) Measured mass growth rate, *dGfm/dt*), as a function of SO_2, NO_2, NH_3, and RH. (*E*) Absorption enhancement (E_{abs}) and *MAC* for fresh and aged BC particles. (*F*) Single-ion monitoring of collected particles for the sulfate ion SO_4^- at $m/z = 96$, the bisulfate ion HSO_4^- at $m/z = 97$, and the oxygen adduct of $SO_3O_2^-$ at $m/z = 112$ measured by ID-TD-CIMS. BC particles during the experiments have an initial diameter (D_p) of 100–150 nm.

surface sites, $\{C\text{-}H\}_{red}$, and to form oxidized carbon, $\{C\}_{ox}$, and {HONO} (26),

$$NO_2(g) + \{S\} \rightarrow \{NO_2 \bullet S\} + \{C\text{-}H\}_{red} \rightarrow \{S\} + \{C\}_{ox} + \{HONO\}, \quad [1]$$

where the bracket denotes adsorbed species or surface sites. NH_3 effectively stabilizes {HONO} via the equilibrium with NO_2^-,

$$\{HONO\} + NH_3 + H_2O \leftrightarrow NO_2^- + NH_4^+ + H_2O. \quad [2]$$

The conversion of sulfide to sulfate is subsequently facilitated by {HONO} (27),

$$SO_2(g) + H_2O \leftrightarrow \{H^+\} + \{HSO_3^-\}, \quad [3]$$

$$2\{HONO\} + 2\{HSO_3^-\} \rightarrow 2\{HSO_4^-\} + N_2O(g) + H_2O. \quad [4]$$

The rate-limiting step of this mechanism corresponds to HONO production (i.e., Eqs. **1** and **2**), which explains the strong dependence on NO_2, NH_3, and RH, but weak dependence on SO_2 for the measured sulfate formation (Fig. 3 *A–D*). Previous measurements of NO_2 uptake on BC surfaces showed that coating of organic acids (glutaric acid) significantly increases the uptake coefficient and HONO yield, because organic acids form strong hydrogen-bonded complexes with polar organic molecules from the occupying $\{C\text{–}H\}_{red}$ sites (26). Also, sulfuric acid coating was shown not to alter the uptake NO_2 coefficient but to reduce the amount of HONO released (26). In contrast, our work reveals an insignificant effect of sulfate formation on BC particle growth upon exposure to SO_2, NO_2, and NH_3. Since our laboratory experiments are conducted to mimic ambient conditions, the mechanism of BC-catalyzed sulfate formation is applicable to other polluted regions worldwide.

Using the laboratory-derived sulfate growth rate on BC particles (*SI Appendix*, Fig. S2) and the field-measured concentrations of gaseous species and BC (*SI Appendix*, Figs. S3 and S4 and Tables S1 and S2), we quantified sulfate production during pollution episodes in Beijing (Fig. 4). During moderate haze events, the measured sulfate mass concentration by an aerosol mass spectrometer (AMS) (28) increases steadily and reaches a peak mass concentration of about 15 μg m^{-3}. Incorporation of the BC catalytic SO_2 reaction reproduces the measured sulfate mass concentration (Fig. 4*A* and *SI Appendix*, Fig. S5*A*). During heavy haze events, the mass concentration of sulfate increases rapidly to about 60–100 μg m^{-3} (Fig. 4*B* and *SI Appendix*, Fig. S5*B*), while the calculated BC catalytic sulfate formation (17–48 μg m^{-3}) accounts for less than 50% of the measured sulfate production. In our work, fresh BC mass concentrations were estimated from a previously measured ratio of fresh to aged BC particles in Beijing (29), to derive the range of sulfate production rates (Fig. 4 *C* and *D* and *SI Appendix*, Fig. S5). To further gain insight into the role of BC particles in sulfate production, we determined the number and mass fractions of BC-containing aerosols using a single-particle AMS (SP-AMS)

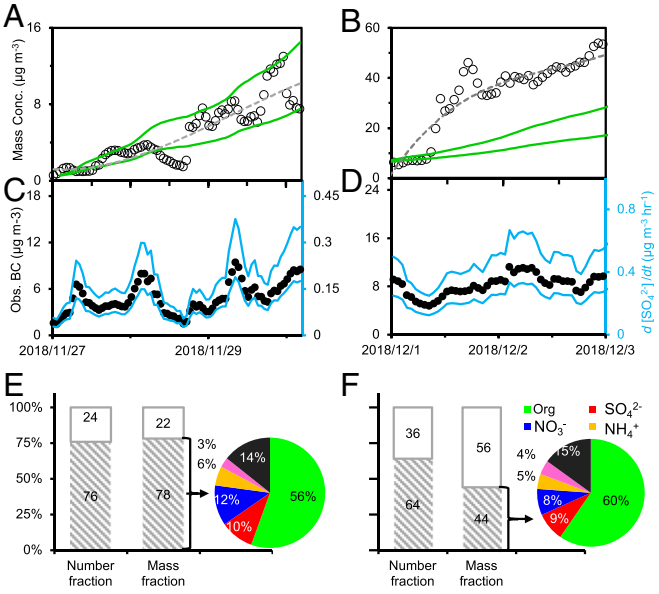

Fig. 4. Quantifying BC-catalyzed sulfate formation. (*A* and *B*) Calculated (green lines) and measured (circles and dashed line) sulfate mass concentrations during a moderate day and a heavy haze day, respectively. (*C* and *D*) BC mass concentration (*Left* axis) and sulfate formation rate ($d[SO_4^{2-}]/dt$, *Right* axis) during a moderate haze day and a heavy haze day, respectively. The ranges of sulfate mass concentration (green lines in *A*) and sulfate formation rate (blue line in *B*) are derived by assuming that 20% and 40% of the measured BC mass concentration are freshly emitted (34). The peak $PM_{2.5}$ and sulfate mass concentrations for the two episodes (27–30 November 2018 and 1–3 December 2018) are 154.0 and 14.2 μg m^{-3} and 330.0 and 55.8 μg m^{-3}, respectively. (*E* and *F*) Number and mass fractions of BC-containing and non-BC particles in ambient $PM_{2.5}$ during moderate and heavy haze events, respectively. The mass fraction of BC-containing particles are derived according to our field-measured BC mass concentrations and previous measurements of mass fraction of each species in BC-containing particles (represented by the pie charts) by a combined single-particle SP2 and AMS during typical moderate and heavy haze days in urban Beijing (37). The number concentration is measured from February 1 to March 11, 2019, during which the moderate and heavy haze events correspond to $PM_{2.5}$ mass concentrations of 160.2 and 355.0 μg m^{-3} and BC mass concentrations of 10.4 and 17.8 μg m^{-3}, respectively.

and a combined SP2 (single-particle soot photometer) and AMS (*Methods*), respectively. During moderate haze events, the number and mass fractions of BC-containing particles are 76% and 78%, respectively, showing significant BC presence (Fig. 4*E*). Using the measured mass fraction of BC-containing particles from SP2-AMS, along with the $PM_{2.5}$ mass concentration and the mass fraction of BC particles, we derived a sulfate concentration of about 12 μg m^{-3}, consistent with that measured by AMS (Fig. 4*A*). During heavy haze events, the number and mass fraction of BC-containing particles are 64% and 44% (Fig. 4*F*), respectively. The derived sulfate concentration of 13 μg m^{-3} is much smaller than that measured by AMS (Fig. 4*B*). Hence, the BC catalytic sulfate production accounts dominantly (about 90–100%) and non-negligibly (about 30–50%) for sulfate production during the moderate and heavy haze events, respectively. The coexistence of BC, sulfate, nitrate, and organics (Fig. 4 *E* and *F*) on $PM_{2.5}$ also implies a mutually promoting mechanism among the various aerosol ingredients to produce high levels of $PM_{2.5}$ (4, 13). In particular, formation of hygroscopic sulfate is essential to drive multiphase chemistry of other aerosol species (1).

Radiative Transfer Calculations

Using a radiative transfer model (30), we quantified the variations of the direct radiative forcing (Δ*DRF*) with and without inclusion of this BC catalytic chemistry on the top of atmosphere (TOA), in the atmosphere (ATM), and at the surface (SFC) (Fig. 5*A* and *SI Appendix*, Fig. S6). The model simulations show nearly invariant TOA Δ*DRF* values of 0.3, 2.1, and 3.4 W m^{-2} from clean/light haze, moderate haze, to heavy haze days, respectively, indicating that the positive ATM Δ*DRF* is nearly offset by negative SFC Δ*DRF*. On the other hand, the BC-catalyzed sulfate formation causes large heating in ATM and large cooling at SFC. The Δ*DRF* values range from 38.3, 126.8, to 175.9 W m^{-2} and from −38.0, −124.8, to −172.6 W m^{-2}, respectively, from clean/light, moderate, to heavy haze days. The large increases in ATM heating and SFC cooling during the haze evolution are attributed to increased coating by sulfate (Figs. 4 *E* and *F* and 5*B*), which substantially increases *MAC* or E_a for BC particles (Fig. 3*E*). The large ATM and SFC Δ*DRF* values also indicate significant atmospheric stabilization, which exacerbates accumulation of $PM_{2.5}$ within the PBL (Fig. 5*C*) (4, 10). Air stagnation is clearly reflected from the measured PBL height, which decreases from 1 to 2 km on clean/light haze days to below 0.5 km on heavy haze days (Fig. 5*C* and *SI Appendix*, Fig. S7). The BC-induced air stagnation imposes strong feedbacks to haze formation and evolution (1, 10). Note that the Δ*DRF* results in our work likely represent a lower bound, since the radiative forcing is expected to be enhanced by coating of other non-BC materials, i.e., nitrate and organics, in addition to sulfate (16). Clearly, the topic of aging and variations in the optical properties and radiative forcing associated with the BC-catalyzed sulfate formation warrants further investigation.

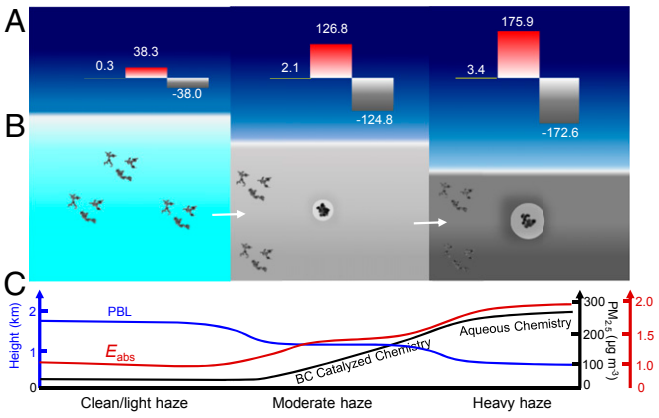

Fig. 5. BC-catalyzed chemistry on regional haze. (*A*) Calculated (Δ*DRF*) of aged BC particles at the TOA, yellow), in the atmosphere (ATM, red), and at the surface (SFC, gray) during clean/light haze, moderate haze, and heavy haze events. The initial fresh BC diameter is ∼150 nm. The colored boxes denote the vertical extends of the free troposphere (dark blue) and the PBL (light blue, gray, or dark gray) during haze evolution from clean/light haze, moderate haze, and heavy haze events, respectively. (*B*) Schematic representation of the morphology evolution from fresh to aged BC particles because of the BC-catalyzed reaction, which significantly impacts light absorption. (*C*) Evolution in the PBL height, absorption enhancement (E_{abs}), and $PM_{2.5}$ mass concentration driven by the BC-catalyzed and aqueous sulfate formation (13, 14). The green, red, and black colors correspond to PBL height, E_{abs}, and $PM_{2.5}$ mass concentration, respectively.

Discussion

Our analysis of long-term measurements of gases and aerosols in NCP shows an improved air-quality trend since 2013, as evident from increasing days of clean/light haze and decreasing days of heavy haze, along with a significantly decreased SO_2 (Fig. 1). The latter is consistent with implementation of strict air-quality standards in China, particularly associated with reduction in coal burning from power plants, industrial facilities, and winter residential heating (4). However, despite considerably lower levels of SO_2 and reduced (increased) frequency of heavy haze (clean/light haze), heavy haze events with high levels of daily $PM_{2.5}$ and sulfate content persist in recent years, showing little alleviated severity (Fig. 2 *B* and *C*). In addition, moderate haze occurs annually on about 30% of the days between 2004 and 2018, with no reduced frequency or sulfate level.

Haze development in China is characterized by rapid sulfate formation (Fig. 2*B*). SO_2 oxidation occurs through gas-phase oxidation or aqueous reactions, but the detailed chemical mechanisms remain controversial (1, 3, 4). The gas-phase oxidation of SO_2 is slow, with a corresponding lifetime of about 1 wk at typical tropospheric levels of hydroxyl radicals (1). For example, the relatively long lifetime of SO_2 was invoked as an explanation for significantly reduced SO_2 emission but without a commensurate reduction in aerosol pollution in the eastern United States (31). Also, atmospheric measurements revealed rapid sulfate production during severe haze events in China (1, 3, 4, 13), which cannot be explained by current atmospheric models (4) and suggests missing sulfur oxidation mechanisms (13).

Our work offers explanations for the puzzling trends of regional haze from the long-term measurements in China (Fig. 5). Haze formation in NCP involves two distinct secondary processes, i.e., new particle formation and growth (1, 2, 13). During haze evolution from clean to polluted conditions, photochemistry is considerably inhibited because of reduced UV radiation by aerosols (13, 32, 33). While new particle formation is mainly driven by photochemistry and occurs consistently under clean conditions (1, 2), rapid particle growth under polluted conditions requires efficient multiphase chemistry (1, 2, 14). Our work unravels a sulfate formation mechanism: SO_2 oxidation is efficiently catalyzed by BC in the presence of NO_2 and NH_3, even at low SO_2 levels (down to a few ppb) and an intermediate RH range (30–70%). This BC catalytic pathway accounts for about 90–100% and 30–50% of sulfate formation during moderate and heavy haze events in Beijing, respectively. Sulfate formation enhances BC aging and light absorption, leading to atmospheric stabilization (Fig. 5 *A* and *B*). Also, BC-containing particles likely engage in coagulation growth with nucleation-mode particles, which consist dominantly of secondary organics (1, 2, 34), to further contribute to BC aging and light absorption (16). On the other hand, our results indicate that this BC catalytic reaction yields only a modest sulfate amount. Other mechanisms, such as the aqueous SO_2 oxidation by NO_2 with NH_3 neutralization

(13, 14, 35), are necessary to account for large sulfate formation during heavy haze events. The BC-catalyzed sulfate formation represents the most critical step to increase aerosol hygroscopicity and aqueous chemistry for secondary aerosol formation, i.e., sulfate, nitrate, and organics (1, 4, 13, 14). Furthermore, air stagnation caused by BC light absorption traps moisture within PBL (4), as evident from considerably increased RH, i.e., from <30%, 30–60%, to 60–90% during the evolution from clean/light haze, moderate haze, to heavy haze conditions, respectively (Fig. 2*C*). Elevated RH results in a positive feedback to multiphase chemistry to further enhance BC-catalyzed and aqueous SO_2 oxidation (4).

The current air-pollution status in China corresponds to a significantly reduced SO_2 level, yet still elevated BC, NO_x, and NH_3 levels (Fig. 2 *B* and *C*). Under such a circumstance, BC-catalyzed SO_2 oxidation occurs efficiently and is responsible for no improved trend for moderate haze events in China. Reduced levels of primary gases and aerosols, as reflected by significantly declined SO_2 levels and slightly declined NO_x and BC levels (Fig. 1), from emission control measures in China inevitably prevent achieving the optimal conditions (i.e., NO_x, NH_3, and BC levels as well as RH and air stagnation) for efficient aqueous chemistry to produce high levels of $PM_{2.5}$ and sulfate (13, 14). This likely explains the decreasing frequency of heavy haze events and increasing frequency of clean/light haze days. However, under unfavorable meteorological conditions, the BC-catalyzed sulfate pathway facilitates the transition to aqueous chemistry to produce high levels of $PM_{2.5}$ during heavy haze events, explaining the long-term measurements of no alleviated haze severity in China. Furthermore, the BC-catalyzed sulfate formation results in an invariant TOA radiative forcing of nearly 0 W m^{-2} throughout haze development, leading to little net climatic cooling or warming by regional haze (Fig. 5*A*).

A most recent work indicated significantly a declined annual mean $PM_{2.5}$ concentration in China over the last 5 y because of anthropogenic emission abatements (36), consistent with our analysis of decreasing heavy haze days and increasing clean/light haze days. On the other hand, our results reveal no alleviated haze severity and little improved trend for moderate haze events, despite lower SO_2 levels and reduced frequency of heavy haze events. We conclude that the BC-catalyzed chemistry plays a dominant role in driving the formation, trend, and radiative forcing of regional haze, highlighting the necessity of simultaneous reduction in emissions of SO_2, NO_x, NH_3, and BC for air-quality improvement.

Methods

Field Measurements. Field measurements were performed to measure the nonrefractory $PM_{2.5}$/chemical components including sulfate (SO_4^{2-}), nitrate (NO_3^-), ammonium (NH_4^+), chloride (Cl), and organics (Org) by a $PM_{2.5}$-Q-ACSM during 11 November to 20 December 2018 in Beijing and Gucheng, which is a suburban site about 120 km south of Beijing. At the both sites, a seven-wavelength aethalometer (model AE33, Magee Scientific Corp.) was used to measure BC. BC Measurements using different methods typically yielded variable results, because of lack in standards (37). For example, measurements by the aethalometer could suffer from interference from non-BC coatings (16). Gaseous species of NO_2 and SO_2 were measured by gas analyzers (ECOTECH). In Beijing, gaseous NH_3 was measured using a cavity ring-down spectrometer (Picarro G2103). The number fractions of BC-containing particles were measured during February 1 to March 11, 2019 by an SP-AMS (Hexin, Inc.) (38). The mass fraction of BC-containing particles was derived according to field measurements of chemical composition of BC-containing particles by a combined single-particle SP2 and AMS (39). The long-term sulfate mass concentration in submicrometer particles during 2011–2018 was measured at the Institute of Atmospheric Physics, Chinese Academy of Sciences in Beijing (40). The concentrations of SO_2, NO_2, and $PM_{2.5}$ during 2009–2012 were measured on the campus of Peking University (2), and the data during 2013–2018 were measured at a site (Wanliu) close to the campus of Peking University (http://beijingair.sinaapp.com/). The NH_3 measurements during winter 2016–2018 were collected using a NH_3 analyzer (Ecotech 9842, Australia) on the campus of China Meteorological Administration. Long-term trends of BC and NH_3 were taken from previously published measurements (41–43). The PBL height during 11–12 January of 2019 in urban Beijing was retrieved from Raman Lidar measurements (44).

Laboratory Experiments. The laboratory experiments were conducted by exposing seed particles to SO_2, NO_2, and NH_3 at variable RH and measuring the dry size variation and sulfate formation on the exposed particles in a 1.2-m^3 Teflon reaction chamber covered with aluminum foil as described previously (13, 14). BC particles from incomplete combustion of propane were heated by a thermal denuder to 300 °C to remove coated organics and then were continuously sampled, diluted, dried, and size-classified by a differential mobility analyzer (DMA) (3081, TSI). The BC density generated from propane combustion in our laboratory experiments was 0.5–0.6 g cm^{-3}, which is within the range of ambient measured density for fresh BC particles in Beijing (16, 18, 22, 30) and representative of fresh BC in the atmosphere. An integrated instrument including the DMA, an aerosol particle mass analyzer (APM, 3600, Kanomax), a condensation particle counter (3760A, TSI), and a thermal denuder was used for measurements of the particle size and mass. A commercial Nephelometer (TSI, 3563) and a cavity ring-down spectrometer was used to measure optical properties, as described elsewhere (45). The chemical composition of the exposed particles was measured by a TD-ID-CIMS (13, 24, 25). The particle mass growth factors (*Gfm*) are expressed as m_p/m_0, respectively, where m_0 and m_p are the particle mass before and after aging. The material density of particles is calculated using those for BC and sulfate (ρ_{BC} = 1.77 g cm^{-3}, ρ_{sul} = 1.77 g cm^{-3}). The particle absorption (E_{abs}) cross-sections were derived by dividing the corresponding optical coefficient by particle number concentration. The TD-ID-CIMS was used to measure sulfate formation on BC. The m_p and m_0 were determined from the size of BC particles measured by DMA and APM, respectively. When determining sulfate formation on BC particles, the bulk measured BC mass concentration by the Aethalometer was used by assuming size-independent mass growth on BC particles due to sulfate formation according to our laboratory results, which showed similar growth for 100- and 150-nm BC particles.

Parameterization of BC-Catalyzed Sulfate Formation from Laboratory Experiments. Based on the laboratory results, we derived an exponential parameterization for the mass growth rate, denoted as *dGfm/dt*, which was used to calculate ambient sulfate production rate from measured trace gases concentrations and RH as follows:

$$\frac{dGfm}{dt} = A[SO_2]^{\alpha}[NO_2]^{\beta}[NH_3]^{\gamma}[f(RH)]^{\delta} + v,$$

where $[SO_2]$, $[NO_2]$, and $[NH_3]$ are the concentrations of gaseous SO_2, NO_2, and NH_3 respectively. We employed a polynomial function f(RH) to parameterize the RH dependence of the laboratory results shown in Fig. 2*D*,

$$f(RH) = -1.61[RH]^2 + 2.51[RH] - 0.34,\ 0 < RH < 100\%.$$

We derived the power exponential constants of α, β, γ, and δ using the power exponential relationship for each variable according to *dGfm/dt* ($dGfm/dt = f(X) = a_i[X_i]^n$), where a_i is the coefficient and $[X]$ is the concentration of the gas precursor, with $n = \alpha$, β, γ, or δ. *A* is a prefactor constant derived from the linear fit of *dGfm/dt* and the product of the power exponential for each variable. An iteration method was further applied to locate the residual *v* value, which is the average of the differences of experimentally measured *dGfm/dt* and the fitted *dGfm/dt* calculated from *A*, $[SO_2]^{\alpha}$, $[NO_2]^{\beta}$, $[NH_3]^{\gamma}$, and $[f(RH)]^{\delta}$. We obtained the following relationship between the gaseous concentrations and RH (>30%):

$$\frac{dGfm}{dt} = 0.1 \times 10^{-3}[SO_2]^{0.01}[NO_2]^{1.01}[NH_3]^{0.46}[f(RH)]^{1.0} + 0.12.$$

The parameterization to estimate the growth rate was evaluated by comparing with the experimental measurements, showing the growth rate with a slope and correlation coefficient of 1.03 and 0.87, respectively, between the predicted and experimental values (*SI Appendix*, Fig. S3). Since the concentrations of 7–750, 37–750, and 100–1,000 ppb for the gaseous SO_2, NO_2 and NH_3, respectively, in our laboratory experiments are close to the ambient levels, this parameterization is applicable broadly to atmospheric models. On combining the observed BC mass concentration and the laboratory results,

the rate of sulfate formation (d [SO_4^{2-}]/d t in μg m^{-3}·h^{-1}) and sulfate mass concentration are calculated by

$$\frac{dSO_4^{2-}}{dt} = [BC]_{fresh} \times \frac{dGfm}{dt},$$

$$f(t) = \sum_{i=0}^{i=t} \left(\frac{dSO_4^{2-}}{dt} \right).$$

Only the episodes with stable meteorological conditions were selected for the estimation. In this study, we assumed that 20% and 40% of the observed BC particles are freshly emitted, to derive the upper and lower limits, respectively (29).

Calculations of Radiative Forcing. The Mie theory with the core–shell assumption for homogeneous spherical particles was used to calculate *MAC* (46). Because the core–shell Mie model assumes that all particles are compact and both the BC core and outer shell are homogeneous, the core of aged BC particles is represented as the mass-equivalent diameter (D_{me}) of fresh BC particle (44). For aged BC particles, the size distribution of the core (D_{core}) is equal to the size distribution of the mass-equivalent diameter of fresh BC particle ($D_{me,0}$). With the assumption that the increases of mass-equivalent diameter (ΔD_{me}) are identical for BC particles within the entire size range, the mass-equivalent diameter of aged BC particles is calculated by adding $D_{me,0}$ and $\Delta D_{me,0}$. With an insignificant organics fraction for fresh BC particles (<30%) during the experiments, we adopted a refractive index of 1.75 + 0.44i for fresh BC particles to determine E_{MAC}. Since the analysis of particle composition by TD-ID-CIMS indicates the presence of dominant sulfate as the coating materials in our experiments, the refractive index of coating sulfate used in this study is 1.60–0.13i (47). The ΔDRF for TOA, ATM, and SFC due to BC-catalyzed sulfate formation is calculated and evaluated by using the Santa Barbara DISORT Atmospheric Radiative Transfer model (30).

Data and Materials Availability. All data needed to evaluate the conclusions in the paper are present in the paper and/or the *SI Appendix*. Additional data related to this paper may be requested from the authors.

ACKNOWLEDGMENTS. This work was supported by the National Natural Science Foundation of China (Grants 41675141 and 41975174), the National Basic Research Program of China (Grant 2017YFC1501702), and the Robert A. Welch Foundation (Grant A-1417). We thank Zipeng Dong for assistance with the radiative forcing data analysis.

1. R. Zhang *et al.*, Formation of urban fine particulate matter. *Chem. Rev.* **115**, 3803–3855 (2015).
2. S. Guo *et al.*, Elucidating severe urban haze formation in China. *Proc. Natl. Acad. Sci. U.S.A.* **111**, 17373–17378 (2014).
3. Y. Wang *et al.*, Enhanced sulfate formation during China's severe winter haze episode in January 2013 missing from current models. *J. Geophys. Res.* **119**, 425–440 (2014).
4. Z. An *et al.*, Severe haze in northern China: A synergy of anthropogenic emissions and atmospheric processes. *Proc. Natl. Acad. Sci. U.S.A.* **116**, 8657–8666 (2019).
5. World Health Organization (WHO), Air pollution (WHO, 2018). https://www.who.int/health-topics/air-pollution#tab=tab_1. Accessed 1 November 2019.
6. K. A. Rychlik *et al.*, In utero ultrafine particulate matter exposure causes offspring pulmonary immunosuppression. *Proc. Natl. Acad. Sci. U.S.A.* **116**, 3443–3448 (2019).
7. G. Wu *et al.*, Adverse organogenesis and predisposed long-term metabolic syndrome from prenatal exposure to fine particulate matter. *Proc. Natl. Acad. Sci. U.S.A.* **116**, 11590–11595 (2019).
8. Intergovernmental Panel on Climate Change, *Climate Change 2013: The Physical Science Basis* (Cambridge University Press, 2013).
9. Y. Wang *et al.*, Assessing the effects of anthropogenic aerosols on Pacific storm track using a multiscale global climate model. *Proc. Natl. Acad. Sci. U.S.A.* **111**, 6894–6899 (2014).
10. Y. Wang, A. Khalizov, M. Levy, R. Zhang, New Directions: Light absorbing aerosols and their atmospheric impacts. *Atmos. Environ.* **81**, 713–715 (2013).
11. Y. Wang *et al.*, Long-term impacts of aerosols on precipitation and lightning over the Pearl River Delta megacity area in China. *Atmos. Chem. Phys.* **11**, 12421–12436 (2011).
12. C. Li *et al.*, India is overtaking China as the world's largest emitter of anthropogenic sulfur dioxide. *Sci. Rep.* **7**, 14304 (2017).
13. G. Wang *et al.*, Persistent sulfate formation from London Fog to Chinese haze. *Proc. Natl. Acad. Sci. U.S.A.* **113**, 13630–13635 (2016).
14. G. Wang *et al.*, Particle acidity and sulfate production during severe haze events in China cannot be reliably inferred by assuming a mixture of inorganic salts. *Atmos. Chem. Phys.* **18**, 10123–10132 (2018).
15. B. H. Samset *et al.*, Climate impacts from a removal of anthropogenic aerosol emissions. *Geophys. Res. Lett.* **45**, 1020–1029 (2018).
16. J. Peng *et al.*, Markedly enhanced absorption and direct radiative forcing of black carbon under polluted urban environments. *Proc. Natl. Acad. Sci. U.S.A.* **113**, 4266–4271 (2016).
17. Y. Wang *et al.*, Constraining aging processes of black carbon in the community atmosphere model using environmental chamber measurements. *J. Adv. Model. Earth Syst.* **10**, 2514–2526 (2018).
18. C. He *et al.*, Variation of the radiative properties during black carbon aging: Theoretical and experimental intercomparison. *Atmos. Chem. Phys.* **15**, 11967–11980 (2015).
19. H. Xue, A. F. Khalizov, L. Wang, J. Zheng, R. Zhang, Effects of coating of dicarboxylic acids on the mass-mobility relationship of soot particles. *Environ. Sci. Technol.* **43**, 2787–2792 (2009).
20. R. Zhang *et al.*, Variability in morphology, hygroscopic and optical properties of soot aerosols during internal mixing in the atmosphere. *Proc. Natl. Acad. Sci. U.S.A.* **105**, 10291–10296 (2008).
21. J. X. Warner *et al.*, Increased atmospheric ammonia over the world's major agricultural areas detected from space. *Geophys. Res. Lett.* **44**, 2875–2884 (2017).
22. M. Levy *et al.*, Measurements of submicron aerosols in Houston, Texas during the 2009 SHARP field campaign. *J. Geophys. Res.* **118**, 10,518–10,534 (2013).
23. Y. Ma *et al.*, Rapid modification of cloud-nucleating ability of aerosols by biogenic emissions. *Geophys. Res. Lett.* **40**, 6293–6297 (2013).
24. R. Zhang *et al.*, Formation of nanoparticles of blue haze enhanced by anthropogenic pollution. *Proc. Natl. Acad. Sci. U.S.A.* **106**, 17650–17654 (2009).
25. L. Wang *et al.*, Atmospheric nanoparticles formed from heterogeneous reactions of organics. *Nat. Geosci.* **3**, 238–242 (2010).
26. A. F. Khalizov, M. Cruz-Quinones, R. Zhang, Heterogeneous reaction of NO(2) on fresh and coated soot surfaces. *J. Phys. Chem. A* **114**, 7516–7524 (2010).
27. S. B. Oblath, S. S. Markowitz, T. Novakov, S. G. Chang, Kinetics of the formation of hydroxylamine disulfonate by reaction of nitrite with sulfites. *J. Phys. Chem.* **85**, 1017–1021 (1981).
28. L. Y. He *et al.*, Submicron aerosol analysis and organic source apportionment in an urban atmosphere in Pearl River Delta of China using high-resolution aerosol mass spectrometry. *J. Geophys. Res.* **116**, D12304 (2011).
29. Y. X. Zhang *et al.*, Mixing state of refractory black carbon of the North China plain regional aerosol combining a single particle soot photometer and a volatility tandem differential mobility analyzer. *Atmos. Chem. Phys. Discuss.*, 1–27 (2017).
30. P. Ricchiazzi *et al.*, SBDART: A research and teaching software tool for plane-parallel radiative transfer in the Earth's atmosphere. *Bull. Am. Meteorol. Soc.* **79**, 2101–2114 (1998).
31. H. He *et al.*, Response of SO_2 and particulate air pollution to local and regional emission controls: A case study in Maryland. *Earths Futur.* **4**, 94–109 (2016).
32. R. R. Dickerson *et al.*, The impact of aerosols on solar ultraviolet radiation and photochemical smog. *Science* **278**, 827–830 (1997).
33. G. Li, R. Zhang, J. Fan, X. Tie, Impacts of black carbon aerosol on photolysis and ozone. *J. Geophys. Res.* **110**, D23206 (2005).
34. M. Shrivastava *et al.*, Recent advances in understanding secondary organic aerosol: Implications for global climate forcing. *Rev. Geophys.* **55**, 509–559 (2017).
35. J. Xue *et al.*, Efficient control of atmospheric sulfate production based on three formation regimes. *Nat. Geosci.* **12**, 977–982 (2019).
36. Q. Zhang *et al.*, Drivers of improved $PM_{2.5}$ air quality in China from 2013 to 2017. *Proc. Natl. Acad. Sci. U.S.A.* **116**, 24463–24469 (2019).
37. C. D. Zangmeister *et al.*, Characterization and demonstration of a black carbon aerosol mimic for instrument evaluation. *Aerosol. Sci. Technol.* **53**, 1322–1333 (2019).
38. X. Bi *et al.*, Mixing state of biomass burning particles by single particle aerosol mass spectrometer in the urban area of PRD, China. *Atmos. Environ.* **45**, 3447–3453 (2011).
39. J. Wang *et al.*, Characterization of black carbon-containing fine particles in Beijing during wintertime. *Atmos. Chem. Phys.* **19**, 447–458 (2019).
40. Y. L. Sun *et al.*, Long-term real-time measurements of aerosol particle composition in Beijing, China: Seasonal variations, meteorological effects, and source analysis. *Atmos. Chem. Phys.* **15**, 10149–10165 (2015).
41. Q. Liu *et al.*, Temporal variations of black carbon during haze and non-haze days in Beijing. *Sci. Rep.* **6**, 33331 (2016).
42. A. S. Emilenko *et al.*, Long-term variability of air pollution with black carbon in the region of Beijing in autumn periods. *Atmos. Oceanic Opt.* **30**, 550–554 (2017).
43. Z. Y. Meng *et al.*, Characteristics of atmospheric ammonia over Beijing, China. *Atmos. Chem. Phys.* **11**, 6139–6151 (2011).
44. M. Lv *et al.*, Retrieval of cloud condensation nuclei number concentration profiles from lidar extinction and backscatter data. *J. Geophys. Res.* **123**, 6082–6098 (2018).
45. C. Qiu, A. F. Khalizov, R. Zhang, Soot aging from OH-initiated oxidation of toluene. *Environ. Sci. Technol.* **46**, 9464–9472 (2012).
46. C. F. Bohren, D. R. Huffman, *Absorption and Scattering of Light by Small Particles* (Wiley Interscience, New York, 1983).
47. G. Lesins, P. Chylek, U. Lohmann, A study of internal and external mixing scenarios and its effect on aerosol optical properties and direct radiative forcing. *J. Geophys. Res.* **107**, 4094 (2002).